sensors

MDPI

Type of the Paper: Article

Power Gain from Energy Harvesting Sources at high MPPT Sampling Rates

Manel Gasulla[1] and Matias Carandell[1]

[1] Electronic Engineering Department, Universitat Politècnica de Catalunya, C/ Jordi Girona 31, 08034 Barcelona, Spain
* Correspondence: manel.gasulla@upc.edu; Tel.: +34 934137092

Abstract: Energy harvesting (EH) sources require tracking their maximum power point (MPP) to ensure maximum energy is captured. This tracking process, performed by an MPP tracker (MPPT), is performed by periodically measuring the EH transducer's output at a given sampling rate. The harvested power as a function of the sampling parameters has been analyzed in a few works, but the power gain achieved with respect to the case of a much slower sampling rate than the EH source's frequency has not been assessed so far. In this work, simple expressions are obtained that predict this gain assuming a Thévenin equivalent for the EH transducer. It is shown that the power gain depends on the relationship between the square of ac to dc open circuit voltage of the EH transducer. On the other hand, it is proven that harvested power increases using a suitable constant signal for the MPP voltage instead of tracking the MPP at a low sampling rate. Experimental results confirmed the theoretical predictions. First, a function generator with a series resistor of 1 kΩ was used emulating a generic Thévenin equivalent EH. Three waveform types were used (sinus, square and triangular) with a dc voltage of 2.5 V and ac rms voltage of 0.83 V. A commercial MPPT with a fixed sampling rate of 3 Hz was used and the frequency of the waveforms was changed from 50 mHz to 50 Hz, thus effectively emulating different sampling rates. Experimental power gains of 11.1 %, 20.7 % and 7.43 % were respectively achieved for the sinus, square and triangular waves, mainly agreeing with the theoretical predicted ones. Then, experimental tests were carried out with a wave energy converter (WEC) embedded into a drifter and attached to a linear shaker, with a sinus excitation frequency of 2 Hz and peak-to-peak amplitude of 0.4 g, in order to emulate the drifter's movement under a sea environment. The WEC provided a sinus-like waveform. In this case, another commercial MPPT with a sampling period of 16 s was used for generating a slow sampling rate whereas a custom MPPT with a sampling rate of 60 Hz was used for generating a high sampling rate. A power gain around 20% was achieved in this case, also agreeing with the predicted gain.

Keywords: Energy harvesting; maximum power point tracking (MPPT); power gain; power management unit; wireless sensor.

Citation: To be added by editorial staff during production.

Academic Editor: Firstname Lastname

Received: date
Revised: date
Accepted: date
Published: date

1. Introduction

Wireless sensors are key components of the Internet of Things [1]. They are commonly powered by primary batteries although energy harvesting (EH) has proven to be a reasonable alternative. Batteries account for a simple design but their energy is limited [2]. Contrariwise, energy harvesters provide unlimited energy, reducing the maintenance and associated costs of battery-powered wireless sensors, at the expense of a more complex design. Mainly, a power management unit (PMU) is required to adapt the random nature of the EH transducer to a constant and clean output and to control the mismatch of energy between the transducer and the wireless sensor.

One key block of PMUs is the maximum power point tracking (MPPT) module [3], which aims to extract maximum power from the EH transducer. It consists of a power converter and a tracking algorithm. The power converter mainly consists of a dc-dc converter but, for ac signals, e.g. those coming from mechanical or radiofrequency transducers, a previous ac-dc rectifier is required. The tracking algorithm provides the reference required to fix the output voltage of the EH transducer (or that of the rectifier) at its maximum power point (MPP).

Two widespread MPPT algorithms are the fractional open circuit voltage (FOCV) and the Perturb and Observe (P&O). The FOCV is based on the ratio (k) between the MPP voltage (v_{MPP}) and the open circuit voltage (OCV) of the EH transducer, e.g. 0.5 for thermoelectrical generators and between 0.7-0.8 for solar cells. FOCV methods are usually implemented by periodically opening the EH transducer for a (short) sampling time (t_{SAMP}), measuring its OCV, and fixing the new v_{MPP}. This technique is simple but the true MPP is not assured. Contrariwise, the P&O performs the periodic measurement of the EH transducer's output power. The true MPP is achieved at the cost of increased complexity. Anyhow, a periodic measurement at a given sampling period (T_s) is required in these and other methods. Its inverse ($f_s = 1/T_s$) is defined as the MPPT sampling rate.

The sampling rate must be high enough to follow the fluctuation of the EH source to continuously place the EH transducer at its MPP. Light and thermal sources usually are slowly varying. On the other hand, mechanical sources, e.g. vibrations, can have relatively fast fluctuations. For example, [4] and [5] present a wind energy harvester (WEH) and a wave energy converter (WEC) respectively, each with the OCV oscillating at around 1.8 Hz. WECs are commonly used to expand the autonomy of free-floating monitoring buoys (e.g. drifters) and many of them have been recently reported. Reference [6] describes an electromagnetic converter that captures energy from the relative motion between a drogue and a drifter, achieving tens of milliwatts of average power in a simulation test. Reference [7] presents an electromagnetic-based swing body that achieved power peaks of 0.13 W under real waves of 0.8 m height. A small-sized, pendulum-type and electromagnetic-based WEC was reported in [8], harvesting energy from a 20 cm diameter drifter, achieving an average useful power of 0.2 mW. These studies show the potential of electromagnetic converters as a promising approach to generate energy from ocean waves as long as the MPP of its oscillating output is tracked fast enough.

Most of the commercial MPPT-based integrated circuits (ICs) use techniques based on the simple FOCV method, with a T_s of several seconds, so not appropriate for these fast-varying EH sources. As an example, the BQ25504/5 (*Texas Instruments*) and the ADP5091/2 (*Analog Devices*) are two of the most widely-used ICs. Their dc-dc converters are very efficient (>80 %) and work in a wide range of powers (from μW to mW) from low input voltages (<100 mV). However, T_S is fixed to 16 s, which is too slow for fast-varying EH sources. Conversely, there are several academic proposals where the sampling rate is high enough. References [9] and [10] use the FOCV method for PV sources, reporting T_s values of 100 ms and 3.33 ms, respectively. Reference [11] examines a vibrational EH source that employs a piezoelectric device, with the PMU refreshing the FOCV-MPPT after the PZT voltage rectification step with T_s = 1 s. In [12], a boost converter is used to harvest energy from PV cells using the FOCV method with very low input voltages and T_S = 150 ms. Reference [13] presents a FOCV technique with an adaptative sampling period that can be reduced down to 4 ms. Other fast-tracking MPPT methods have also been reported as that presented in [14], where the P&O method have been used for PV sources to feed wireless sensor nodes.

Nevertheless, few works have analyzed the harvested power in function of the sampling parameters. In [15], the sampling parameters are optimized for the FOCV and the P&O methods to maximize the power harvested from resonant piezoelectric vibration harvesters (RPVH) after an ac-dc bridge rectification step. Expressions are provided and experimentally validated for a 153.6 Hz sinusoidal acceleration whose amplitude is modulated by a 50 s period saw-tooth waveform with acceleration ranging from 0.75 g to 1.25 g. For the FOCV method, an optimum T_s of 16.7 s with a t_{SAMP} of 0.3 s results. An approximate analytical expression is provided in [16] for the harvested power with the FOCV method and considering a sinusoidal waveform for the EH transducer. It is shown that, for negligible sampling times, the larger the sampling rate, the larger the harvested power, and that 99 % of the maximum power can be obtained with a sampling rate just 15 times that of the EH transducer's frequency. On the other hand, the same as in [15], a trade-off exists for non-negligible sampling times resulting in an optimum sampling rate. Experimental tests made with a WEC under simulated sea condition were also performed.

Nonetheless, to the best of our knowledge, no work in the literature theoretically estimates the power gain achieved by sampling at high rates with respect to the case of low sampling rates. For this, it is necessary to tackle both the favorable case when f_s is much higher than the EH source frequency (f_o), i.e. $f_s >> f_o$ (high sampling rate), as well as the unfavorable case when $f_s << f_o$ (low sampling rate) and thus the harvested power decreases. This paper provides in both cases simple expressions for the harvested power of time-varying EH sources, assuming they can be modelled as a Thévenin equivalent, and the corresponding power gain. On the other hand, it is demonstrated that more power can be harvested by setting a suitable constant value for v_{MPP} instead of tracking the MPP at a low sampling rate. Experimental results corroborate the analytical findings. First, a function generator (FG) was used to emulate a generic Thévenin equivalent EH transducer. Then, an actual WEC attached to a linear shaker provided more realistic results.

2. Theoretical Analysis

The proposed analysis derives the harvested power from EH transducers, both for high and low sampling rates with respect to the frequency of the EH transducer signal (f_s/f_o), and the corresponding power gain that can be achieved. The analysis is circumscribed to EH transducers that can be modelled as a Thévenin (or Norton) equivalent circuit. This is the case, for example, of thermoelectric transducers and dc electrical generators as in [17] and [8], respectively. But also, of radiofrequency [18] and resonant piezoelectric vibration energy harvesters [19] when including the ac-dc rectifier.

Figure 1 shows the Thévenin equivalent circuit of the energy transducer, where v_T is the Thévenin voltage (OCV), R_T the Thévenin resistance, and v_o and i_o the output voltage and current, respectively. It is well known that the output power, $p_o = v_o \times i_o$, can achieve a maximum value whenever the equivalent resistance connected to the output terminals is equal to R_T or equivalently when $v_o = v_{MPP} = v_T/2$ [20]. In this case, p_o is given by

$$p_{\mathrm{MPP}} = v_{\mathrm{T}}^2/4R_{\mathrm{T}} \quad (1)$$

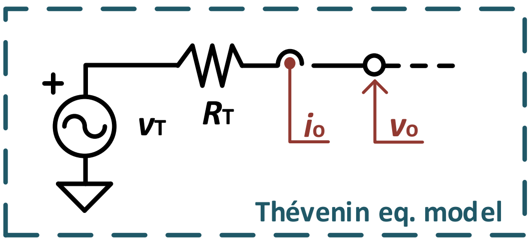

Figure 1. Thévenin equivalent circuit and parameters.

EH source variations will translate to variations in v_T. So, v_T can be expressed as

$$v_{\mathrm{T}}(t) = V_{\mathrm{dc}} + v_{\mathrm{ac}}(t) \quad (2)$$

where V_{dc} and v_{ac} are the dc (average) and ac (time-varying) components of v_T. Substituting (2) in (1) and performing the time average, we get the average of p_{MPP}

$$P_{\mathrm{MPPH}} = \overline{p_{\mathrm{MPP}}(t)} = \frac{V_{\mathrm{dc}}^2 + V_{\mathrm{rms}}^2}{4R_{\mathrm{T}}} = P_{\mathrm{dc}}(1 + \alpha^2) \quad (3)$$

where $V_{\rm rms}$ is the rms voltage of $v_{\rm ac}$, $P_{\rm dc} = V_{\rm dc}^2/4R_{\rm T}$ and $\alpha = V_{\rm rms}/V_{\rm dc}$. $V_{\rm dc}$ can take positive and negative values whereas $V_{\rm rms}$ only positive values. So α can take any positive or negative value, becoming infinite for $V_{\rm dc} = 0$. For the particular case in which $v_{\rm ac}$ is a sinus, triangular, or square signal, $V_{\rm rms}$ is $V_{\rm p}/\sqrt{2}$, $V_{\rm p}/\sqrt{3}$, or $V_{\rm p}$, respectively, where $V_{\rm p}$ is the peak voltage of $v_{\rm ac}$.

To fix the MPP, an MPPT algorithm must be used, e.g. FOCV or P&O, that periodically samples $v_{\rm T}$ (every $T_{\rm s}$). Figure 2 shows an illustrative example where $v_{\rm T}$ is represented as a sinus with positive offset and period $T_{\rm o}$ (=1/$f_{\rm o}$). Also shown is the corresponding $v_{\rm MPP}$ (=$v_{\rm T}$/2) together with the resulting $v_{\rm o}$ for high ($T_{\rm s} \ll T_{\rm o}$) and low sampling rates ($T_{\rm s} \gg T_{\rm o}$). As can be seen in both cases, $v_{\rm o}$ is fixed to $v_{{\rm MPP},i} = v_{{\rm T},i}/2$ each $T_{\rm s}$ (the subindex i indicates the sampling number), whereas $v_{\rm T}$ keeps varying.

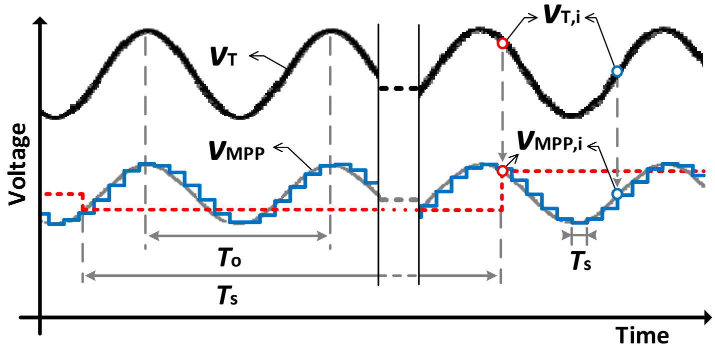

Figure 2. Sinusoidal-shape, time-varying $v_{\rm T}$ signal and the corresponding $v_{\rm MPP}$ (=$v_{\rm T}$/2) together with the resulting $v_{\rm o}$ for two sampling rates: $T_{\rm s} \ll T_{\rm o}$ (blue solid line) and $T_{\rm s} \gg T_{\rm o}$ (red dashed line).

The result in (3) is achieved for the case of high sampling rates. In [16], it is shown that 99 % of the maximum power is achieved for $f_{\rm s} = 15f_{\rm o}$. For any waveform type, (3) is achieved whenever $f_{\rm s} \gg f_{\rm omax}$, being $f_{\rm omax}$ the maximum frequency component of $v_{\rm ac}$. On the other hand, for low sampling rates and assuming, for the sake of simplicity, $T_{\rm s}$ an integer multiple of $T_{\rm o}$, the average of $p_{\rm MPP}$ within $T_{\rm s}$ will be

$$\overline{p_{{\rm MPP},i}(t)} = \frac{1}{T_{\rm s}}\int_{T_{\rm s}} v_{{\rm MPP},i}\left(v_{\rm T}(t) - v_{{\rm MPP},i}\right)/R_{\rm T} = v_{{\rm MPP},i}\left(V_{\rm dc} - v_{{\rm MPP},i}\right)/R_{\rm T} \quad (4)$$

This expression is valid for any $v_{\rm T}$ periodic signal. The value of (4) depends on the sampled value $v_{{\rm MPP},i}$. Zero values are achieved for $v_{{\rm MPP},i}$ equal to 0 or $V_{\rm dc}$ ($v_{{\rm T},i}$ equal to 0 or $2V_{\rm dc}$) and even negative values surpassing these limits, whenever the excursion range of $v_{\rm T}$ allows it. Differentiating (4) with respect to $v_{{\rm MPP},i}$ and equating it to zero, we get $v_{{\rm MPP},i} = V_{\rm dc}/2$ ($v_{{\rm T},i} = V_{\rm dc}$), for which power is maximum and equal to

$$\overline{p_{{\rm MPP},i}(t)} = P_{\rm dc} \quad (5)$$

Yet, this maximum value is lower than (3) since the sampled value is held constant and not following the pace of $v_{\rm T}$.

In a realistic scenario, $T_{\rm s}$ will not be a multiple of $T_{\rm o}$ and $v_{{\rm MPP},i}$ will take values within the full range of $v_{\rm T}$/2. In the long term, all the instants within a period $T_{\rm o}$, where the measurements every $T_{\rm s}$ are performed, are equiprobable. Thus, the overall average of $p_{\rm MPP}$ can be obtained performing the time average of (4), resulting in

$$\overline{p_{\rm MPP}(t)} = \overline{\overline{p_{{\rm MPP},i}(t)}} = \frac{\overline{V_{\rm T}\left(V_{\rm dc} - \frac{V_{\rm T}}{2}\right)}}{2R_{\rm T}} = P_{\rm dc}(1 - \alpha^2) \quad (6)$$

where $v_{MPP,i}$ has been substituted by $v_T/2$, and v_T is given by (2). The result of (6) can be extrapolated to any waveform type as long as $f_s \ll f_{omin}$, where f_{omin} is the minimum frequency component of v_{ac}.

As can be seen, (3) is higher than (6). This means that using low sampling rates decreases the harvested power. In fact, for $\alpha > 1$, (6) becomes negative, which means that the EH transducer, in average, would drain power instead of producing it. The value of (5) is also higher than (6). So, whenever the sampling rate cannot be conveniently increased, a better strategy is to fix v_{MPP} to $V_{dc}/2$ to achieve (5). Moreover, (4) is also higher than (6) whenever

$$(V_{\text{dc}} - V_{\text{rms}})/2 < v_{\text{MPP},i} < (V_{\text{dc}} + V_{\text{rms}})/2 \tag{7}$$

However, the knowledge of V_{dc} (and V_{rms}) requires a previous characterization of the EH source and transducer. To assess the benefit of increasing the sampling rate, a normalized power gain factor (G_P) is defined as the difference between (3) and (6) divided by P_{dc},

$$G_{\text{p}} = \frac{P_{\text{MPPH}} - P_{\text{MPPL}}}{P_{\text{dc}}} = 2\alpha^2 \tag{8}$$

The value of P_{dc} can also be obtained as the average of P_{MPPH} and P_{MPPL}. Whenever v_T is a purely dc signal, i.e. V_{rms} and thus α are zero, (3) and (6) are equal to P_{dc} and $G_P = 0$, so that no power gain is achieved by operating at high sampling rates. For $|\alpha|$ increasing, G_p increases and thus using high sampling rates makes sense. The larger $|\alpha|$, the larger the power gain. An infinite value of $|\alpha|$ and G_p is achieved for $V_{dc} = 0$, i.e. for v_T with no dc value, because P_{dc} becomes zero.

3. Materials and Methods

Two setups and tests were used and performed to validate the analytical findings. First, a FG was used to emulate a generic Thévenin equivalent EH transducer. Then, an actual WEC attached to a linear shaker emulated a drifter's movement under a sea environment.

3.1. Test with a function generator

Figure 3 shows the experimental setup of the first test used to prove the formulation of Section 2. The EH transducer was emulated with a function generator, FG (33210A, Agilent; output impedance of 50 Ω) in series with a resistor of 1 kΩ (R_S); thus, R_T = 1,05 kΩ. As for the MPPT, the evaluation board of the AEM30940 PMU chip (e-peas) was used. It implements the FOCV technique with T_s = 0.33 s (f_s = 3 Hz) and t_{SAMP} = 5.12 ms. The value of k was set to 0.5. A power analyzer, PA (WT310, Yokogawa) was placed between the FG and the MPPT to measure the input power. The PA was programmed with an integration time of 100 s, accounting for 300 samples of the MPPT ($300T_s$). The PMU output (BATT pin) was connected to a Source Measure Unit, SMU (B2901A, Agilent) fixed at 3.9 V.

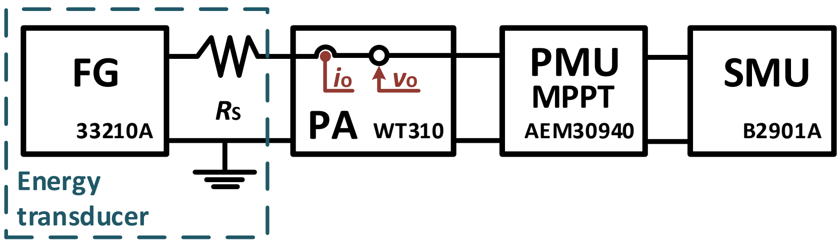

Figure 3. Experimental setup for the test with the function generator.

The MPPT only accepts positive values of v_o and i_o, and so of p_o. Thus, v_T was set positive and its minimum value (v_{Tmin}) higher than the maximum value of $v_{MPP,i}$ (v_{MPPmax}) to keep i_o positive. Hence, the following inequality must be satisfied for periodic signals:

$$v_{\mathrm{Tmin}} = V_{\mathrm{dc}} - V_{\mathrm{p}} > v_{\mathrm{MPPmax}} = \frac{V_{\mathrm{dc}} + V_{\mathrm{p}}}{2} \Rightarrow V_{\mathrm{p}} < V_{\mathrm{dc}}/3 \quad (9)$$

Accordingly, the FG was programed with V_{dc} = 2.5 V and V_P = 0.83 V (α = 0.236). Three waveforms types were used: sinus, square and triangular. Thus, we have P_{dc} = 1.488 mW and for the sine/square/triangular waveforms: P_{MPPH} = 1.571/1.653/1.543 mW from (3), P_{MPPL} = 1.405/1.323/1.433 mW from (6), and G_P = 11.1/22.2/7.41 % from (8). Frequency f_o was swept over 3 decades from 50 mHz (T_o = 20 s) to 50 Hz (T_o = 20 ms) in a sequence 1-2-5-10. The resulting f_s/f_o ranged from 0.06 (low sampling rate) to 60 (high sampling rate).

3.2. Test with a WEC

In [16], experimental tests were carried out with a WEC embedded into a drifter and attached to a linear shaker (APS 129), with an excitation frequency of 2 Hz (f_o), in order to emulate the drifter's movement under a sea environment (Section V.C of [16]**)**. A block schematic and a picture of the experimental setup are shown in Figure 4 and Figure 5, respectively. The electrical model for the WEC matches that of Figure 1. The WEC was attached to the shaker's moving platform with the device's pendulum aligned to the movement axis. The shaker's acceleration was set with a sinus wave of frequency 2 Hz and peak-to-peak amplitude 0.4 g, similar to that reported in [5] from a drifter under sea-

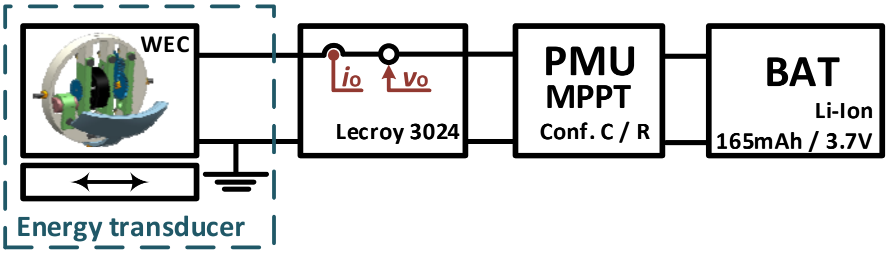

Figure 4. Scheme of the experimental setup for the WEC test.

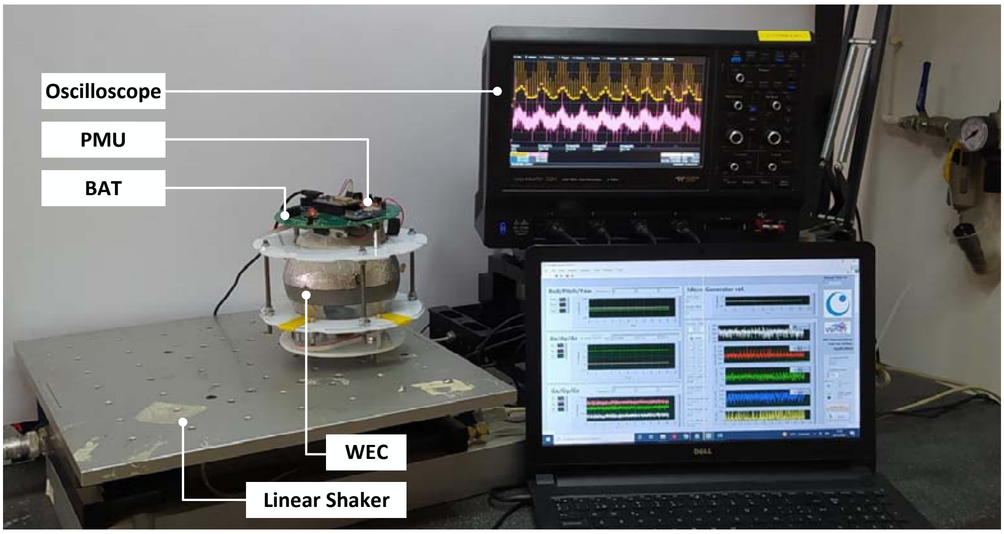

Figure 5. Picture of the experimental setup for the WEC test.

wave excitation. The WEC's output was connected to the PMU. Two MPPT systems were used, both using a FOCV method. First, the commercial ADP5092 IC with a low sampling rate (config. R: f_s = 1/16 Hz = f_o/32). Second, a custom PMU using the ADP5092 IC with additional low-power sampling circuitry to drastically increase the sampling rate with respect to config. R. (config. C: f_s = 60 Hz = 30f_o). A Li-Ion rechargable battery of 165 mAh and 3.7 V was placed as a load at the PMU's output. An oscilloscope (Lecroy Wavesurfer

3024) was used to measure both v_o and i_o (this last one also using a shunt resistor and a current sense amplier as described in [16]). From these parameters input power to the PMU can be estimated. The data obtained in [16] were used here with further processing to validate the equations presented here for high and slow MPPT sampling rates.

4. Results and Discussions

4.1. Test with a function generator

Figure 6 and Figure 7 show, for the sine waveform, oscilloscope screen captures of v_o (in orange) and at the output of the FG (in green) for f_o = 0.1 Hz and f_o = 10 Hz, respectively. The output of the FG nearly provides v_T. In both cases, the sampling process happens every 0.33 s approximately, as previewed, where v_o instantly rises to v_T and then settles to the updated value (v_T/2). For f_o = 0.1 Hz (f_s/f_o = 30) v_o nearly follows v_T/2, whereas for f_o = 10 Hz (f_s/f_o = 0.3) v_o cannot keep the pace of v_T.

Table 1 shows f_o, f_s/f_o and the experimental results of p_o for the three waveform types. As can be seen, p_o approaches the predicted values both for high (f_s/f_o >> 1) and low sampling rates. Experimental values are slightly lower, which can be justified by the non-negligible value of t_{SAMP} with respect to T_s (1.55 %) during which no energy is harvested [16]. In between, a minimum is found around f_s/f_o = 1.5. The experimental values of G_P are obtained from (8) using the power values of the first row as P_{MPPL} and those of the last row as P_{MPPH}. P_{dc} was calculated from the average of these two values. Resulting values are G_P = 11.1/20.7/7.43 %, thus mainly agreeing with the theoretical ones. Larger values of G_P could be achieved by increasing V_P and thus α. However, as stated in Section 3.1, this was not implemented by the limitations of the MPPT chip.

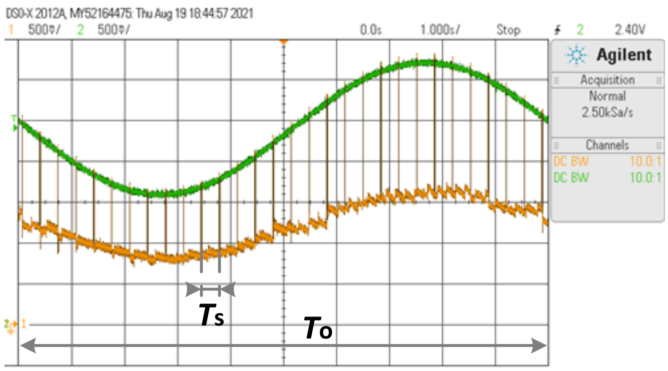

Figure 6. Oscilloscope screen capture for the sine waveform when f_o = 0.1 Hz. CH1: v_o - 500 mV/div, CH2: v_T - 500 mV/div, and time base 1 s/div.

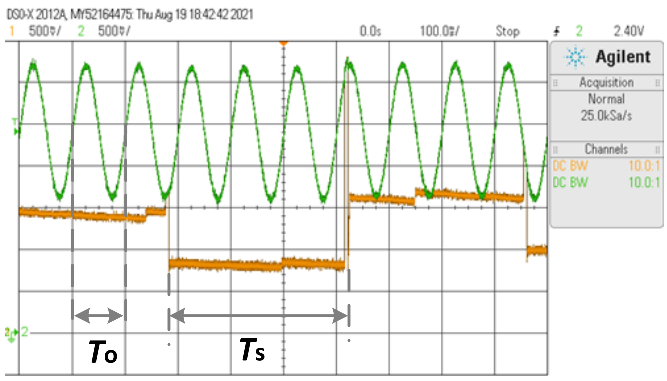

Figure 7. Oscilloscope screen capture for the sine waveform when f_o = 10 Hz. CH1: v_o - 500 mV/div, CH2: v_T - 500 mV/div, and time base 100 ms/div.

Table 1. Experimental values for the test with a function generator.

f_o (Hz)	f_s/f_o	Sinus p_o (mW)	Square p_o (mW)	Triangle p_o (mW)
50	0.06	1.385	1.314	1.412
20	0.15	1.386	1.310	1.412
10	0.3	1.395	1.327	1.418
5	0.6	1.374	1.294	1.406
2	1.5	1.357	1.267	1.395
1	3	1.454	1.417	1.457
0.5	6	1.520	1.527	1.501
0.2	15	1.543	1.589	1.517
0.1	30	1.546	1.609	1.520
0.05	60	1.547	1.617	1.521

4.2. Test with a WEC

Figure 8 shows the measured v_o for the WEC test using configurations C (fast MPPT) and R (slow MPPT). For the fast MPPT, an acquisition window of 5 s was used, whereas for the slow MPPT it was set to 200 s. For the slow MPPT, v_o increases to v_T every T_s = 16 s during t_{SAMP} = 256 ms. In the fast MPPT, the voltage is nearly sinusoidal and corresponds to $V_T/2$. In this case, v_o does not rise to V_T on each sample, as usual, which is a particularity of config. C [16]. From these last data, we can process the values of V_{dc} and V_{rms}, which are 2.006 V and 0.616 V, respectively. Thus, from (3), P_{MPPH} = 8.67 mW, and from (6), P_{MPPL} = 7.17 mW. These values nearly match those experimentally measured in [16] with the fast and slow MPPT systems, 8.66 mW and 6.93 mW, respectively. The corresponding theoretical and experimental values of G_P are 18.9 % and 22.2 %, respectively. So, a good match is also achieved with an actual EH transducer.

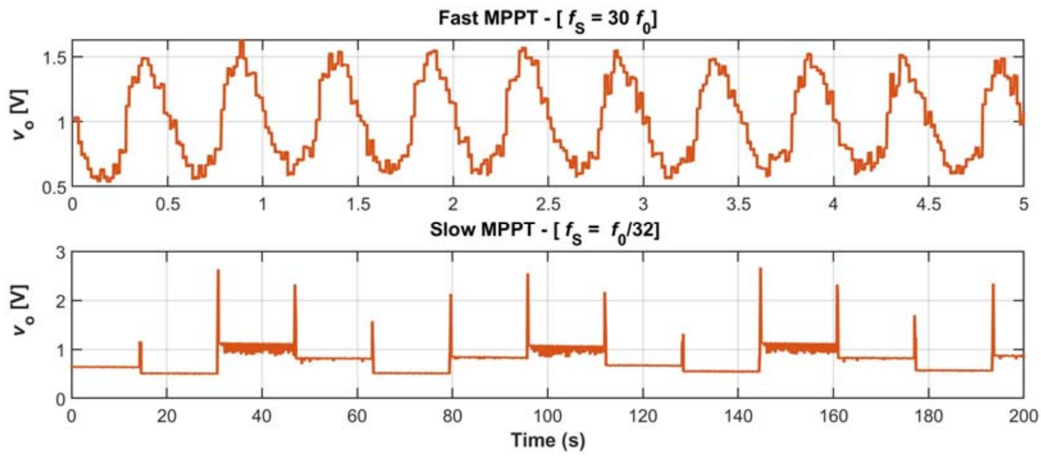

Figure 8. Measured v_o for the WEC test. Top: fast MPPT (config. C). Bottom: slow MPPT (config. R).

4. Conclusions

This work shows that by increasing the sampling rate of MPPTs more power can be extracted from the energy transducers. In particular, the sampling rate should be quite higher, e.g. at least 15-30 times, than the frequency of the EH source. Contrariwise, sampling at low rates, lower than the frequency of the EH source, is detrimental. A normalized power gain factor has been defined resulting in a simple analytical expression, which depends on the relationship of the square of the ac to dc voltage of the EH source, which is assumed as an equivalent Thévenin circuit. Experimental results have confirmed the theoretical predictions. A generic Thévenin equivalent EH source has been emulated using a

FG programmed with sinusoidal, square, and triangular waveform types. The dc voltage was set to 2.5 V and the ac RMS voltage to 0.83 V in all cases. A commercial MPPT system with a sampling rate of 3 Hz has been used to measure the power gains achieved by varying the frequency of the FG across three decades, from 50 mHz to 50 Hz. The power gains obtained have been 11.1%, 20.7%, and 7.43% for sinusoidal, square, and triangular waves, respectively, which are in agreement with theoretical predictions. Additionally, experimental tests have been conducted with a WEC embedded into a drifter and attached to a linear shaker, mimicking the drifter's movement under a sea environment, with an excitation frequency of 2 Hz and a peak-to-peak amplitude of 0.4 g. The WEC provides a sinus-like wave. A commercial MPPT with a sampling period of 16 s has been used to fix a low sampling rate whereas a custom MPPT with a sampling rate of 60 Hz generates a high sampling rate. This results in a power gain of around 20%. Therefore, the expressions presented in the study provide a useful tool for predicting the power gain that can be achieved by choosing an appropriate sampling rate for the MPPT system. This can help to optimize the performance of MPPT systems in future studies.

Author Contributions: "Conceptualization, M.G. and M.C.; methodology, M.G.; software, M.G. and M.C.; validation, M.G. and M.C.; formal analysis, M.G.; investigation, M.G. and M.C.; resources, M.G. and M.C.; data curation, M.G. and M.C.; writing—original draft preparation, M.G. and M.C.; writing—review and editing, M.G. and M.C.; visualization, M.C.; supervision, M.G.; project administration, M.G.; funding acquisition, M.G. All authors have read and agreed to the published version of the manuscript."

Funding: "This work was supported by the European Innovation Council under the EU Horizon Europe program - Grant agreement No 101071179, project SUSTAIN (Smart Building Sensitive to Daily Sentiment)". "The second author was supported by the European Union – NextGenerationEU and the Ministerio de Universidades – Plan de Recuperación, Transformación y Resiliencia under a Margarita Salas post-doctoral research fellowship (ref. 2022UPC-MSC-94068)."

Institutional Review Board Statement: "Not applicable."

Informed Consent Statement: "Not applicable."

Data Availability Statement: -

Acknowledgments: -

Conflicts of Interest: "The authors declare no conflict of interest."

References

1. Khalifeh, A.; Mazunga, F.; Nechibvute, A.; Nyambo, B.M. Microcontroller Unit-Based Wireless Sensor Network Nodes: A Review. *Sensors* **2022**, *22*, 8937, doi:10.3390/s22228937.
2. Callebaut, G.; Leenders, G.; Van Mulders, J.; Ottoy, G.; De Strycker, L.; Van der Perre, L. The Art of Designing Remote Iot Devices—Technologies and Strategies for a Long Battery Life. *Sensors* **2021**, *21*, 913, doi:10.3390/s21030913.
3. Salas, V.; Olías, E.; Barrado, A.; Lázaro, A. Review of the Maximum Power Point Tracking Algorithms for Stand-Alone Photovoltaic Systems. *Sol. Energy Mater. Sol. Cells* **2006**, *90*, 1555–1578, doi:10.1016/j.solmat.2005.10.023.
4. Shi, M.; Holmes, A.S.; Yeatman, E.M. Nonlinear Wind Energy Harvesting Based on Mechanical Synchronous Switch Harvesting on Inductor. In Proceedings of the 21st International Conference on Solid-State Sensors, Actuators and Microsystems (Transducers) - Virtual; IEEE, 2021; Vol. 1, p. ISBN:978-1-6654-1267-4.
5. Carandell, M.; Toma, D.M.; Alevras, P.; Gasulla, M.; del Río, J.; Barjau, A. Nonlinear Dynamic Analysis of a Small-Scale Pendulum-Type Wave Energy Converter for Low-Power Marine Monitoring Applications. In Proceedings of the 14th European Wave and Tidal Energy Conference, EWTEC - Plymouth; 2021; pp. 1–7, ISBN 2706-6940.
6. Harms, J.; Hollm, M.; Dostal, L.; Kern, T.A.; Seifried, R. Design and Optimisation of a Floating Wave Energy Converter for Drifting Sensor Platforms in Realistic Ocean Waves. *Appl. Energy* **2022**, *321*, doi:10.1016/j.apenergy.2022.119303.
7. Li, Y.; Guo, Q.; Huang, M.; Ma, X.; Chen, Z.; Liu, H.; Sun, L. Study of an Electromagnetic Ocean Wave Energy Harvester

Driven by an Efficient Swing Body Toward the Self-Powered Ocean Buoy Application. *IEEE Access* **2019**, *7*, 129758–129769, doi:10.1109/access.2019.2937587.
8. Carandell, M.; Toma, D.M.; Carbonell, M.; del Río, J.; Gasulla, M. Design and Testing of a Kinetic Energy Harvester Embedded into an Oceanic Drifter. *IEEE Sens. J.* **2020**, *20*, doi:10.1109/jsen.2020.2976517.
9. Simjee, F.I.; Chou, P.H. Efficient Charging of Supercapacitors for Extended Lifetime of Wireless Sensor Nodes. *IEEE Trans. Power Electron.* **2008**, *23*, 1526–1536, doi:10.1109/tpel.2008.921078.
10. Shao, H.; Li, X.; Tsui, C.Y.; Ki, W.H. A Novel Single-Inductor Dual-Input Dual-Output DC-DC Converter with PWM Control for Solar Energy Harvesting System. *IEEE Trans. Very Large Scale Integr. Syst.* **2014**, *22*, 1693–1704, doi:10.1109/tvlsi.2013.2278785.
11. Yu, C.G. A Vibrational Energy Harvesting Interface Circuit with Maximum Power Point Tracking Control. *Int. J. Appl. Eng. Res.* **2017**, *12*, 12102–12107.
12. Shrivastava, A.; Roberts, N.E.; Khan, O.U.; Wentzloff, D.D.; Calhoun, B.H. A 10 MV-Input Boost Converter with Inductor Peak Current Control and Zero Detection for Thermoelectric and Solar Energy Harvesting with 220 MV Cold-Start and -14.5 DBm, 915 MHz RF Kick-Start. *IEEE J. Solid-State Circuits* **2015**, *50*, 1820–1832, doi:10.1109/jssc.2015.2412952.
13. Saini, G.; Baghini, M.S. An Energy Harvesting System for Time-Varying Energy Transducers with FOCV Based Dynamic and Adaptive MPPT for 30 NW to 4 MW of Input Power Range. *Microelectronics J.* **2021**, *114*, doi:10.1016/j.mejo.2021.105080.
14. Zhu, X.; Fu, Q.; Yang, R.; Zhang, Y. A High Power-Conversion-Efficiency Voltage Boost Converter with MPPT for Wireless Sensor Nodes. *Sensors* **2021**, *21*, doi:10.3390/s21165447.
15. Balato, M.; Costanzo, L.; Lo Schiavo, A.; Vitelli, M. Optimization of Both Perturb & Observe and Open Circuit Voltage MPPT Techniques for Resonant Piezoelectric Vibration Harvesters Feeding Bridge Rectifiers. *Sensors Actuators, A Phys.* **2018**, *278*, 85–97, doi:10.1016/j.sna.2018.05.017.
16. Carandell, M.; Holmes, A.S.; Toma, D.M.; del Río, J.; Gasulla, M. Effect of the Sampling Parameters in FOCV- MPPT Circuits for Fast-Varying EH Sources. *IEEE Trans. Power Electron.* **2022**, *38*, 2695–2708, doi:10.1109/tpel.2022.3216109.
17. Proto, A.; Bibbo, D.; Cerny, M.; Vala, D.; Kasik, V.; Peter, L.; Conforto, S.; Schmid, M.; Penhaker, M. Thermal Energy Harvesting on the Bodily Surfaces of Arms and Legs through a Wearable Thermo-Electric Generator. *Sensors* **2018**, *18*, doi:10.3390/s18061927.
18. Gasulla, M.; Ripoll-Vercellone, E.; Reverter, F. A Compact Thévenin Model for a Rectenna and Its Application to an RF Harvester with MPPT. *Sensors* **2019**, *19*, 1641, doi:10.3390/s19071641.
19. Alghisi, D.; Dalola, S.; Ferrari, M.; Ferrari, V. Triaxial Ball-Impact Piezoelectric Converter for Autonomous Sensors Exploiting Energy Harvesting from Vibrations and Human Motion. *Sensors Actuators, A Phys.* **2015**, *233*, 569–581, doi:10.1016/j.sna.2015.07.020.
20. Thomas, R.E.; Rosa, A.J.; Toussaint, G.J. *The Analysis and Design of Linear Circuits*; 8th ed.; JOHN WILEY & SONS, 2016; ISBN 0471386790.